



## RESEARCH ARTICLE

# First Distance-of-Flight Instrument: Opening a New Paradigm in Mass Spectrometry

Alexander W. G. Graham,<sup>1</sup> Steven J. Ray,<sup>1</sup> Christie G. Enke,<sup>1,2</sup> Charles J. Barinaga,<sup>3</sup> David W. Koppenaal,<sup>3</sup> Gary M. Hieftje<sup>1</sup>

<sup>1</sup>Department of Chemistry, Indiana University, Bloomington, IN, 47405, USA

<sup>2</sup>Department of Chemistry, University of New Mexico, Albuquerque, NM, 87131, USA

<sup>3</sup>Pacific Northwest National Laboratory, Richland, WA, 99352, USA

## Abstract

A new instrumental concept, distance-of-flight mass spectrometry (DOFMS), is demonstrated experimentally. In DOFMS the mass-to-charge ratio of ions is determined by the distance each ion travels during a fixed time period; the mass spectrum is then recorded with a position-sensitive detector. The DOF approach provides a new way to separate and quantify components of complex samples. Initial results are demonstrated with a glow discharge ion source and a microchannel plate–phosphor screen detector assembly for atomic ion determination. This detection system demonstrated mass spectral peak widths of approximately 0.65 mm, corresponding to resolving powers of approximately 400–600 for a number of elemental samples.

**Key words:** Mass spectrometry, Instrumentation, Glow discharge

Since the development of the first mass spectrograph over 90 years ago [1], numerous methods and instruments have been developed to separate and determine ions of varying mass-to-charge ratio ( $m/z$ ). Currently, mass spectrometry (MS) can be accomplished by electrostatic and magnetic dispersion (sector-field MS), radio-frequency stability and filtering (quadrupoles and ion traps), resonance frequency determination (Fourier-transform ion cyclotron resonance and Orbitrap® MS), or velocity-based separation (time-of-flight MS). These mature MS technologies are routinely employed in a range of applications from biomolecule analysis to elemental isotope determination, and are often coupled with each other to achieve tandem MS analysis [2, 3]. In the present paper, we describe the first implementation of a new form of MS, termed distance-of-flight mass spectrometry (DOFMS), and suggest potential benefits of this new mass separation technique.

Distance-of-flight mass spectrometry is akin to time-of-flight mass spectrometry (TOFMS) in that both techniques separate ions of different  $m/z$  based upon an imparted  $m/z$ -dependent velocity. In TOFMS, each ion is given the same energy (thus achieving a  $m/z$ -dependent velocity), and the  $m/z$  of each ion is calculated from the time required for it to traverse a known distance to a single detector. Conversely, in DOFMS the  $m/z$  of an ion is measured based on the spatial location of each ion at a specific time after the initial acceleration. As a useful analogy, DOFMS is to TOFMS as thin-layer chromatography is to elution chromatography (e.g., LC). TOFMS measures ions as they come off the “column”, whereas DOFMS measures how far the ions travel after a specific separation time. Whereas TOFMS disperses ions in time, DOFMS disperses ions in space.

The principle behind DOFMS is illustrated in Figure 1. To implement DOFMS, the primary ion beam is introduced into an orthogonal extraction region where ions are subjected to a brief electrostatic field, imparting identical momentum to each ion. This constant-momentum acceleration (CMA) is accomplished by limiting the temporal width and electrostatic field

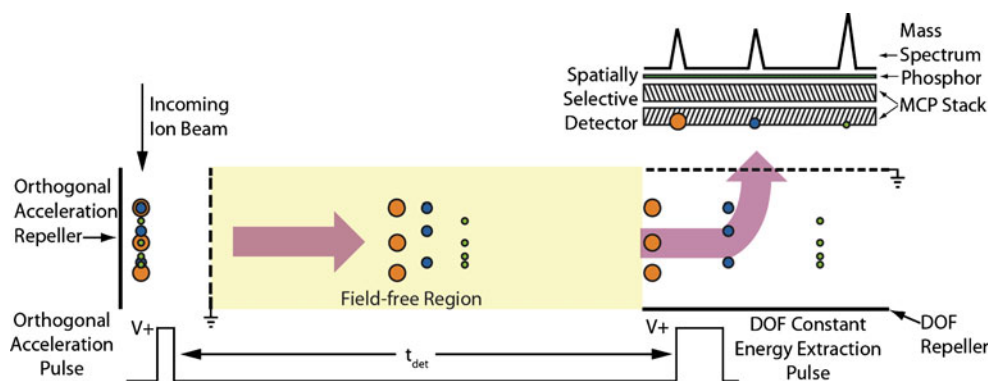


**Figure 1.** Schematic diagram illustrating the operating principle of DOFMS. Ions are electrostatically pushed to a constant momentum along a direction orthogonal to the incoming ion beam. Once within the field-free region, ions separate according to their mass-dependent velocities (ions of larger  $m/z$  are represented by bigger circles). At a given detection time ( $t_{det}$ ), ions are collectively accelerated onto a position-selective detector via a constant-energy voltage pulse applied to the DOF repeller electrode. In our current instrument, a microchannel plate (MCP)–phosphor detector is employed to determine ion position at  $t_{det}$ . The DOF recorded is inversely related to  $m/z$ .

strength of the CMA pulse so that no ions exit the extraction region before the CMA pulse terminates [4]. The extracted ion packet is then allowed to drift through a field-free region where ions separate according to their  $m/z$ -dependent velocities. At a specific detection time ( $t_{det}$ ) delayed from the CMA pulse, the  $m/z$ -separated ions are collectively accelerated by a second electrostatic field oriented orthogonally to their drift axis. This second electrostatic pulse is of longer duration, subjecting all ions to a constant-energy acceleration (CEA) onto the surface of a position-sensitive ion detector. The position at which an ion of given  $m/z$  strikes the detector correlates with the distance traversed by an ion during this analysis time and is inversely proportional to the  $m/z$  of the ion [5].

Realization of DOFMS requires ions of all  $m/z$  to be focused at a single instant, at which time their positions can be measured to produce a mass spectrum. Energy-focusing conditions for DOFMS were mathematically derived by Enke and Dobson [5]. They found that by incorporating a simple linear-field reflection, ions of *all*  $m/z$  could be energy-focused at a single instant known as the energy focus time (EFT). Importantly, this EFT is a function of the electric field within the reflectron and the magnitude of momentum imparted to the ions; thus, the EFT can be controlled electronically to focus different mass ranges sequentially onto a single, stationary, spatially-selective detector. Equation 1 is used to calculate the EFT,

$$EFT = \frac{4\tau E_p}{E_R} \quad (1)$$

where  $\tau$  is the constant-momentum acceleration (CMA) pulse width,  $E_p$  is the CMA electric field strength, and  $E_R$  is the reflectron electric field strength. Although the initial kinetic energy of ions in the CMA region is corrected with a linear-field reflectron, the spatial dispersion of ions prior to their extraction remains constant throughout the flight path.

Like TOFMS, DOFMS is a velocity-based mass separation technique and thus offers a number of advantages over alternative MS approaches. Namely, TOFMS and DOFMS both have theoretically unlimited mass ranges, can generate thousands of complete mass spectra per second, and are simple in design and construction. For these reasons, TOFMS instruments are emerging as analyzers of choice for complex chromatographic detection [6]. DOFMS, however, also enjoys several potential advantages over TOFMS that stem from detecting ions distributed in space, as opposed to detecting their temporal distribution at a single point. First, fast detectors and analog-to-digital converters (ADCs) requisite to high-resolution TOFMS are limiting due to both performance and high cost [7]—DOFMS obviates the need for such devices. Further, by distributing ion flux across a number of discrete detectors, pulse pile-up issues often troublesome in TOFMS are alleviated. In addition, the possible incorporation of discrete charge-detector arrays [8, 9] offers substantial dynamic range improvements over state-of-the-art TOFMS detector technology, while also reducing mass bias inherent to current TOFMS detection [10, 11]. In both DOFMS and TOFMS ions arrive at the detectors intermittently as ion bunches are accelerated out of the source region. However, with DOFMS and a charge-detector array, the signal does not have to be collected and processed for each bunch; the signal from any number of ion bunches can accumulate on the detector between readouts of the charge. The duty factor in DOFMS can reach unity depending on the mass range analyzed. Finally, because DOFMS is a spatially dispersive technique, the possibility exists for simultaneous non-destructive collection of several ions of interest (with essentially no upper mass limit). To date, spatially dispersive MS has been achieved with sector-field instruments that are limited by magnetic-field requirements for high-mass analysis and the physical limitations as to detector arrangement and placement.

In the present work, the first experimental realization of DOFMS is reported. A glow discharge ion source is used to produce atomic ions, which are then separated according to DOFMS principles and imaged onto a position-sensitive ion detector. The field-free flight path of this instrument is just 30 cm. Results from this proof-of-principle instrument demonstrate the feasibility of DOFMS, and demonstrate a mass resolving power greater than 400 (at full width at half maximum, FWHM) for a number of atomic elements. A glow discharge was employed for the detection of atomic ions predominantly because of its simple, reliable design and the resulting straightforward mass spectra. However, DOFMS as a mass separation method is amenable to all ion sources currently available, including molecular ion sources. In fact, planar ion sources such as matrix-assisted laser desorption/ionization (MALDI) or secondary ion mass spectrometry (SIMS) are particularly well suited to DOFMS because they produce ions with a defined spatial distribution—work toward coupling DOFMS to alternative ion sources is underway. In our current instrumental configuration, the particular detector type employed limits instrument performance, so future development of DOFMS detectors and applications are being considered.

## Instrument Design and Experimental

Our proof-of-principle DOFMS instrument was constructed in-house, with the mass analysis chamber machined from a single block of aluminum with Viton® o-ring sealed aluminum caps. Figure 2 depicts a mechanical drawing of the instrument with the pathway of an accelerated ion packet through the instrument highlighted. The instrument consists of a glow discharge ion source, differentially pumped vacuum interface, a set of direct current (DC) quadrupole ion optics to shape the input beam, constant-momentum acceleration region, field-free drift region, single-stage linear-field ion reflectron, and DOFMS detection region. The DOFMS detector assembly lies atop the field-free region and is viewed from above through a vacuum viewport.

### Glow Discharge Ion Source

Atomic ions were generated by a direct current, reduced-pressure argon glow discharge (GD) between an energized conductive sample and a grounded anode [12]. The metal sample being analyzed served as the GD cathode and was fixed by an o-ring seal to an anode with a 9.5-mm-diameter orifice; the distance between the cathode and anode was 0.5 mm. A controlled flow of argon (>99% purity, Airgas Inc., Radner, PA) was bled into the GD chamber (1st vacuum stage) via a needle valve to maintain a constant pressure of 0.7 Torr. The GD operating potential was typically  $-1000$  V, supporting a current of 10 mA. Non-standardized steel, brass, bronze, and lead samples were obtained from the Edward G. Bair Mechanical Services

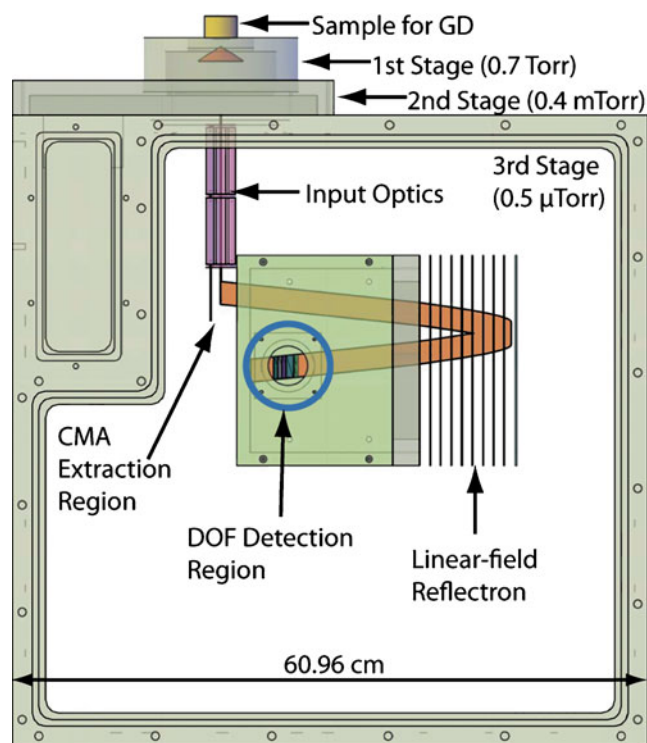


Figure 2. Mechanical drawing of DOF instrument with ion flight path shown in orange.

Facility in the Chemistry Department of Indiana University and held by vacuum against the GD interface to serve as analytes for proof-of-principle studies.

### Vacuum System

Ions were introduced into the mass analysis chamber via a differentially pumped interface. The glow discharge chamber (1st stage) was evacuated with an Edwards E2M30 rotary-vane pump (Edwards, Crawley, UK). A LECO® nickel skimmer cone with 1-mm orifice separated the 1st and 2nd stages of the vacuum system. A pressure of 0.4 mTorr was maintained in the 2nd vacuum stage with an Edwards EXT250H turbomolecular pump backed by an Edwards RV3 rotary-vane pump. The mass analysis chamber (3rd stage) was separated from the 2nd stage by a conductance-limiting orifice (1 mm diameter) and a pressure of  $0.5 \mu\text{Torr}$  was maintained in the 3rd stage with an Edwards STP 451 turbomolecular pump backed by an Edwards RV12 rotary-vane pump.

### Ion Optics

Ions generated with the GD were transmitted into the mass analysis stage with an extraction optic (S1) located behind the skimmer and prior to the third-stage orifice. Within the mass analysis chamber, the ion beam was shaped and focused by a DC quadrupole doublet that was previously described [13, 14]. The doublet consists of four ring

electrodes (designated 1, 2, 3, and 4), two sets of quadrupole rods (X1, Y1, X2, Y2), and a slit electrode. The optics stack begins with two ring electrodes, followed by the first quad set, the third ring electrode, the second quad set, the fourth ring electrode, and finally the slit electrode. The slit electrode contained a vertical slit 5 mm in width. Typical operating potentials are provided in Table 1.

### *Constant-Momentum Acceleration and Field-Free Drift Region*

After transmission and focusing of the primary ion beam, ions were orthogonally accelerated into a field-free region. Constant-momentum acceleration was achieved by electrostatically pulsing a repeller plate to create a time-dependent linear acceleration field in the CMA region short enough that all ions are still within the extraction region at the cessation of the pulse [4]. The CMA region was 22.86 mm long; a +500 V, 1  $\mu$ s nominally square voltage pulse was applied to the CMA repeller to achieve CMA extraction (high voltage pulser—DEI GRX, Directed Energy, Inc., Boulder, CO; high voltage power supply—Bertan 210-01R, Bertan Associates, Inc., Hicksville, NY). The repetition rate of the CMA pulse was typically 10 kHz. Timing was controlled by a BNC 556 pulse generator (Berkeley Nucleonics Corporation, San Rafael, CA) operated remotely under LabVIEW® (version 8.6, National Instruments, Austin, TX) control. Following CMA extraction, ions drift according to their spontaneous drift trajectories [15] through a 30-cm field-free region and turn around in an 11-cm linear-field reflectron.

### *Distance-of-Flight Extraction and Detection*

Distance-of-flight detection was achieved by applying a time-delayed constant-energy acceleration field to selectively push bunches of  $m/z$ -separated ions upward onto an MCP-phosphor detector assembly (see Figure 3). This orthogonal DOF acceleration region was centered at a field-free flight distance 30 cm from the CMA region, 12.6 cm from the exit of the ion reflectron. The physical dimensions of the spatially selective detector are an important aspect of the design. As is shown in Figure 3b, the ion beam passed

**Table 1.** Operating conditions for ion optics in DOFMS instrument

Electrostatic optic	Operating voltage (V)
S1	-800
1	-277
2	0
X1	-412
Y1	-416
3	0
X2	-215
Y2	-219
4	0
Slit	-64

through the center of a 10-mm-wide CEA extraction region and the surface of the MCP-phosphor detector was positioned 10 mm above the grounded DOF extraction region electrode. This detector location corresponded to the position of the space-focus plane, a well-described consequence of CEA and often employed in TOFMS [16]. By using space focusing along this vertical extraction dimension of the DOFMS detector, isomass ions that were initially distributed across the width of the CEA region were made to arrive at the detector surface at the same time after CEA extraction. In this way, the otherwise detrimental effect of the initial ion-packet width on the DOFMS mass spectral resolution was minimized [5]. This space focus condition was reinforced with a grounded slit electrode, 5 mm in width and positioned immediately prior to the DOFMS region; this slit electrode was used to restrict the initial width of the ion packet to the center of the CEA region. Typical CEA extraction consisted of a +3000 V pulse applied for 2  $\mu$ s (high voltage pulser—DEI PVX-4140; high voltage power supply—Bertan 205B-03R) delayed by 15–45  $\mu$ s from the CMA pulse, depending on the  $m/z$  range to be analyzed.

The MCP-phosphor detection assembly comprised two 25-mm-diameter MCP plates (Photonis USA, Inc, Sturbridge, MA) stacked in the chevron configuration. A metalized phosphor screen (4-cm active area, P43 phosphorescent compound, Beam Imaging Solutions INC., Mead, CO) was positioned 2.5 mm above the top MCP. The MCP stack was operated with -1700 V at the front MCP and ground potential on the back MCP; a voltage divider compensated for resistance mismatch of the two MCPs and power was supplied by a Bertan 205A-05R high voltage power supply. The phosphor screen was biased to +3000 V with a Bertan 205-30B supply.

### *Mass Spectrum Acquisition*

In order to obtain a DOF mass spectrum, an optical image of the DOFMS lines appearing on the phosphor plate was captured photographically. Quantitative images of DOF mass spectra were recorded with an intensified charge-coupled device (ICCD) camera (512  $\times$  512 pixels, PiMax 2, Roper Scientific, Inc., Trenton, NJ) fitted with a conventional camera lens (AF Nikkor,  $F=50$  mm,  $f/1.8$ , Nikon Inc., Torrance, CA) through a Plexiglas® viewport positioned directly above the DOF detector. A digital SLR camera (Canon Rebel XT) was also used to capture qualitative images. Line spectra were extracted from the ICCD image by generating 15 line profiles of intensity vs. pixel number with Origin® (OriginPro 8.1, OriginLab Corporation, Northampton, MA) software and averaging these line profiles.

## **Results and Discussion**

The DOFMS instrument was initially characterized by recording isotopic distributions of several singly charged atomic ions across the elemental mass range. These mass

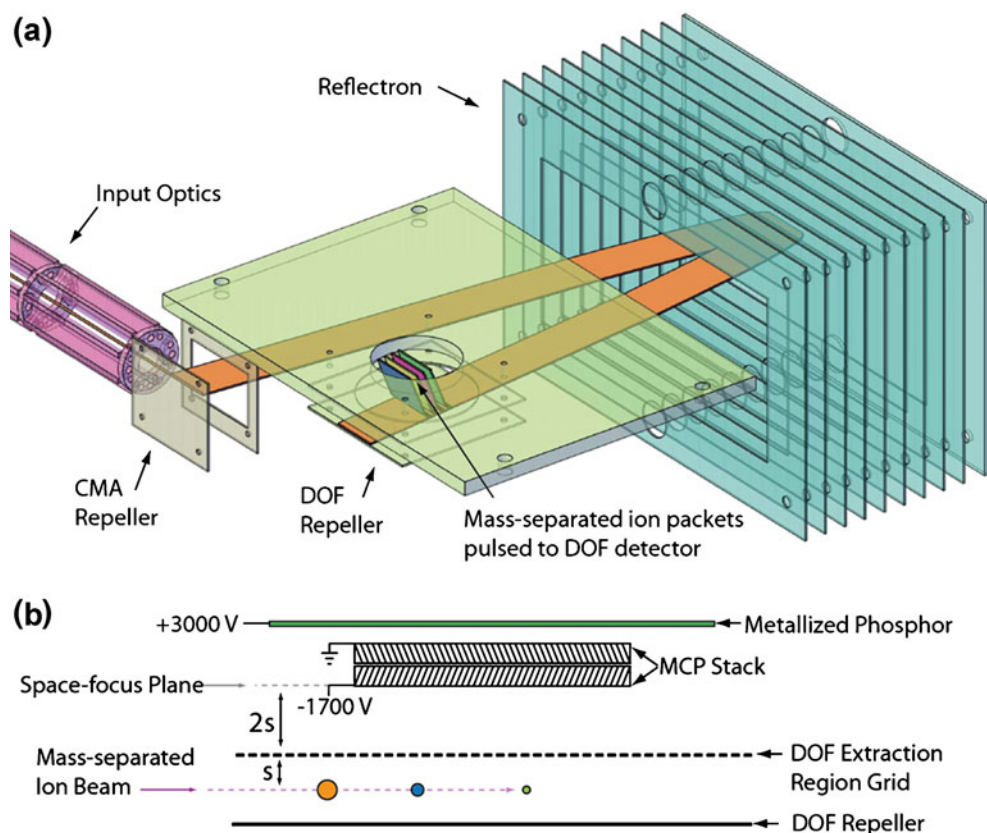


**Figure 3.** (a) Illustration of DOF instrument with ion beam highlighted in orange. After CMA extraction and turnaround in a linear-field reflectron, ions are focused at a single EFT. Slightly before this EFT, a constant-energy acceleration (CEA) pulse pushes the  $m/z$ -separated ions upward onto a spatially selective ion detector (not shown). (b) Side-on schematic diagram of the DOF extraction region. The MCP-phosphor detection assembly is at a position of  $2s$  from the CEA region.

spectra were recorded by imaging the phosphor screen through a viewport located directly above the DOF detection assembly. Photographs of a typical DOFMS spectrum and MCP-phosphor assembly under ambient light are shown in Figure 4a. Unfortunately, the diameter of the available MCPs limited the observable region of the DOFMS spectrum to a

single 25-mm-diameter circle at any given time, covering a field-free flight distance from 287.5 mm to 312.5 mm at the extremes. However, the entire DOFMS spectrum is in focus at the same instant (at the EFT), and would be available for analysis with a physically larger detector. The DOFMS spectral lines are more apparent in Figure 4b in the absence of external illumination. Here, each vertical line represents a tin isotope with a relative intensity that corresponds to the natural isotopic abundance. The spatial distribution of the DOFMS spectral lines also illustrates the inverse relationship between flight distance and  $m/z$ , with the lighter isotopes observed at progressively longer flight distances.

The present DOFMS detector assembly is of limited size and lies at a fixed location along the ion flight axis. Thus, in this proof-of-principle instrument, conditions must be changed to bring ions of varying  $m/z$  to focus on the detector surface. The delay time between the CMA and DOFMS extraction events, the reflectron field, and the CMA field were adjusted according to Eq. 1 to bring a desired mass range into focus at the detector [5]. Several examples of atomic DOFMS mass spectra obtained from a variety of GD samples are shown in Figure 5. The false-color DOFMS images representing the isotopes of chromium (Figure 5a), copper and zinc (Figure 5b), tin and antimony (Figure 5c),

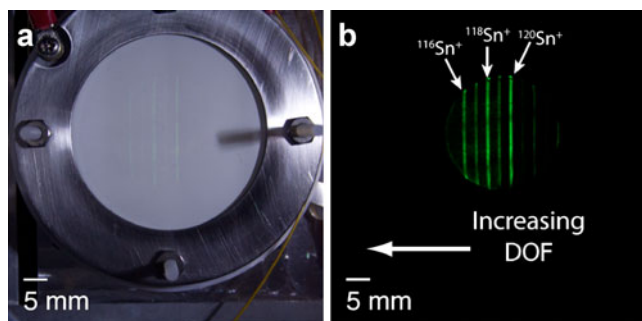


**Figure 4.** Photographs of MCP-phosphor assembly illuminated with white light (a), and without background light (b) taken with a digital camera. Images were captured through a Plexiglas® viewport directly above DOF detection region. The DOFMS lines in Figure 4b represent the isotopes of tin from glow discharge of a bronze sample.

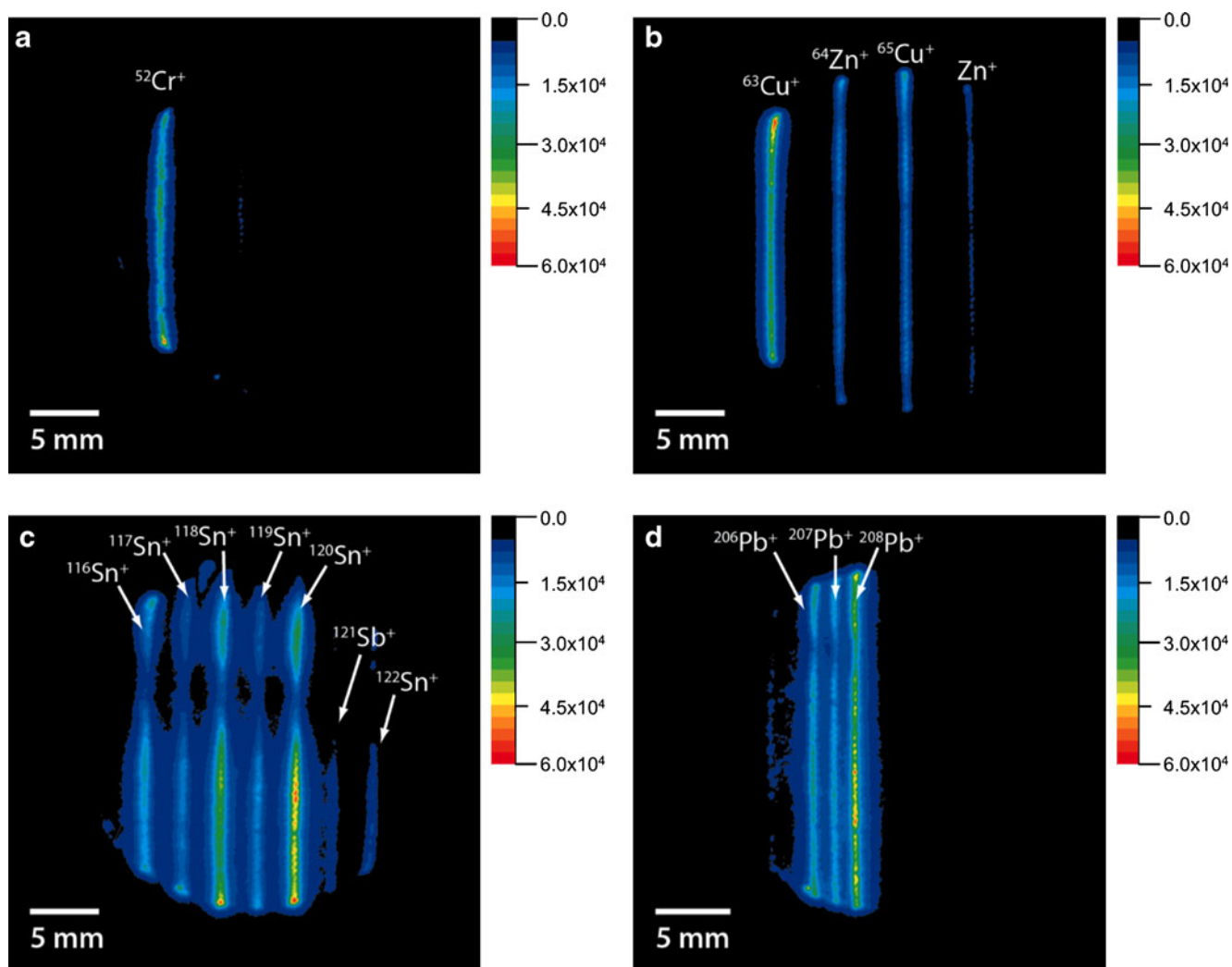


Figure 5. DOF mass spectral images measured with the MCP–phosphor detector and imaged with an ICCD camera. Mass spectra cover the elemental mass range with isotopes of chromium (a) from a steel sample, the isotopes of copper and zinc from a brass sample (b), the isotopes of tin from a bronze sample (c), and the isotopes of lead (d). Different mass ranges were focused at the stationary DOF detector at detection times of 19.8, 25.19, 23.6, and 44.6  $\mu\text{s}$  for (a), (b), (c), and (d) respectively.

and lead (Figure 5d) generally show well-formed vertical slit images, with the inverse proportionality of distance and  $m/z$  evident in the interspacing of the isotopes. A very slight curvature of the lines and subtle variations in intensity along the length of the line were also observed. The DOFMS line curvature is likely due to inadvertent focusing of the electrons between the MCP plate and phosphor screen, and is most severe near the edges of the MCPs. The variation in intensity along the DOFMS lines might be a consequence of spatial variation in phosphor response, or small variations in the grid material of the ion reflectron and the field lensing and focusing that occurs at these points. Further, the size of the ion packet that is extracted is slightly larger than the dimensions of the detector, and lateral spreading of the ion packet that takes place during the ion flight certainly leads to variation in intensity of the lines along their length.

For these reasons, a small section of 15 horizontal pixel rows (1 mm) along the detector midline was used to generate

line-profile plots from each DOFMS image in order to determine the peak shape and mass resolution. Figure 6 presents  $m/z$ -calibrated line-profile plots of DOFMS images from Figure 5. Line plots were calibrated with a linear fit of DOF vs.  $(m/z)^{-1}$  and are plotted on a linear scale. A closer examination of the  $^{63}\text{Cu}^+$  isotope (Figure 6b) reveals a width of 0.62 mm at FWHM, representing a mass resolving power of  $R_{(\text{FWHM})}=588$ . While the shape of the DOFMS peak fits well to a Gaussian distribution over the high-abundance portion of the curve, the peak shows a significant pedestal that results in poor abundance sensitivity. A potential disadvantage of the current DOFMS design is that the space-focusing techniques used in TOFMS cannot be exploited to reduce the spatial width of the ion packet at the detector surface. The peak width and therefore the resolution are largely determined by the initial spatial distribution of ions within the CMA extraction region. In our current design, the DC quadrupole assembly and slit

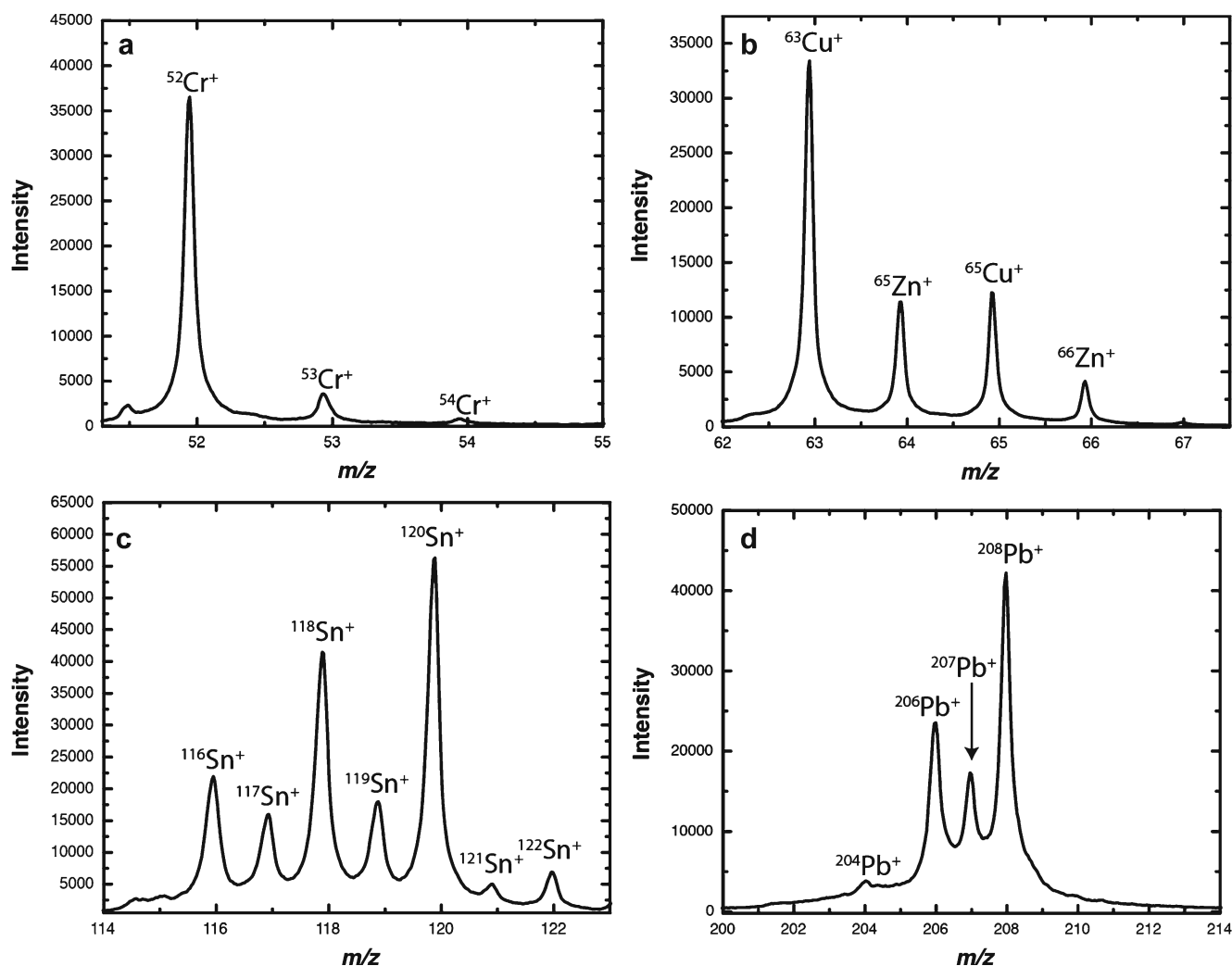


Figure 6. DOFMS mass spectral line profiles corresponding to the DOFMS images in Figure 5 presented on a linear  $m/z$  axis

optic are used to limit this initial width while yielding high ion throughput. Imperfect focusing and peak broadening may also stem from field inhomogeneities in the CMA extraction region that prevent isomass ions distributed across the source from receiving a constant momentum. To minimize unwanted field gradients, a series of uniformly spaced electrodes might be employed to force a linear field across the entire CMA region for the duration of the extraction pulse [4]. Additionally, the high-mass peak tailing apparent in the mass spectra in Figure 6 is a product of second-order energy term fundamental to DOFMS [5]. This tailing can be alleviated by reducing the initial ion energy distribution through use of a cooler ion source such as atmospheric pressure chemical ionization (APCI) or incorporation of collisional cooling prior to DOFMS analysis.

Figure 6 demonstrates measured peak widths of 0.6–1 mm (FWHM) for each isotope and little  $m/z$  dependence is observed, as would be expected. These peak widths correspond to a minimum resolving power of approximately  $R_{(\text{FWHM})}=400$  for ions across the elemental mass range,

which is sufficient to fully resolve isotopes separated by a single mass unit. The characteristic peak shape is also retained for all  $m/z$  investigated, with pedestals that become more evident with increasing  $m/z$ .

The spatial widths of the DOFMS lines observed with the current MCP–phosphor detection system (cf. Figure 6) are a convolution of the actual ion packet width, the secondary electron spread in the MCP stack, the electron spread from the MCP to the phosphor, the resolution of the phosphor, and the resolution of the ICCD camera employed to image the phosphor. Notably, the secondary electron spread through a chevron MCP stack results in as large as a 10-fold increase in electron cloud diameter compared to the impacting ion beam [17].

## Conclusions

Distance-of-flight mass spectrometry represents a new paradigm in mass spectrometry—the spatial dispersion and simultaneous detection of ions of unlimited  $m/z$ . This

technology is well suited for analysis of atomic ions as demonstrated here, but is also primed for the analysis of large molecules and for chromatographic detection.

The MCP-phosphor detector assembly employed in this first implementation of DOFMS dramatically limits instrument performance. Although our MCP-phosphor assembly has proven adequate for demonstrating DOFMS principles, substantial enhancements are expected by employing a flat detector with better sensitivity and spatial resolution. Recently, discrete charge-detector arrays were developed and coupled to sector-field focal plane mass spectrometers [18–20]. These detection systems consist of a linear array of charge-collecting micro-scale Faraday strips with operational amplifiers to integrate and amplify charge resulting from ion strikes, with all components fabricated on a single silicon monolith [21]. Incorporation of such state-of-the-art array detector technology is a natural progression for DOFMS because it enables simultaneous, high-dynamic-range detection on a time scale suitable for chromatographic detection [22]. Specifically, by controlling gain levels of the individual channels across which ion peaks are spread, array detector sensitivities can be adjusted so ion flux differences at least as great as six orders of magnitude could be detectable simultaneously. This broad dynamic range could prove critical for characterization of complex mixtures such as crude oil, whole blood, or other biological samples. In addition, charge detectors are ideal for heavy mass detection because response is proportional solely to ion charge, and they therefore exhibit no appreciable mass bias. Interest in heavy mass detection (and possible collection) includes analysis of moieties such as intact proteins or viruses.

A technological consideration of DOFMS detection is that simultaneous  $m/z$  determination over a broad mass range requires an extended spatially selective detector. Currently, we are characterizing a 2.1-cm-long array of 1696 charge detectors; another group reported development of a 12-cm-long array of 9600 channels [23]. Continued advances in semiconductor fabrication technology should provide DOF detectors of sufficient length to obtain truly simultaneous DOF detection across a wide mass range. The incorporation of existing solid-state spatially sensitive detector technology will lead to complex mass spectral analysis by DOFMS in the near future.

## Acknowledgements

The authors are grateful to the Indiana University Edward G. Bair Mechanical Instrumentation Facility for construction of the DOFMS instrument. This work was supported in part by Laboratory Directed Research & Development (LDRD) funds from Pacific Northwest National Laboratory (operated by Battelle Memorial Institute under contract to the US Department of Energy), by the US Department of Energy through federal grant number DE-FG02-98EF14890, and by the Lilly Endowment-Indiana MetaCyt Initiative.

## References

1. Dempster, A.J.: A new method of positive ray analysis. *Phys. Rev.* **11** (4), 316 (1918)
2. Chernushevich, I.V., Loboda, A.V., Thomson, B.A.: An introduction to quadrupole-time-of-flight mass spectrometry. *J. Mass Spectrom.* **36**(8), 849–865 (2001)
3. McLuckey, S.A., Wells, J.M.: Mass Analysis at the Advent of the 21st Century. *Chem. Rev.* **101**(2), 571–606 (2001)
4. Wolff, M.M., Stephens, W.E.: A Pulsed Mass Spectrometer with Time Dispersion. *Rev. Sci. Instrum.* **24**(8), 616–617 (1953)
5. Enke, C.G., Dobson, G.S.: Achievement of energy focus for distance-of-flight mass spectrometry with constant momentum acceleration and an ion mirror. *Anal. Chem.* **79**(22), 8650–8661 (2007)
6. Enke, C.G.: The unique capabilities of time-of-flight mass analyzers. In: *Adv. Mass Spectrom.*, Elsevier Science Publishers B. V.: Amsterdam, vol. 14, pp 197–219 (1998)
7. Gross, J.H.: *Mass spectrometry: a textbook.* Springer-Verlag, Berlin (2004)
8. Barnes, J.H., Hieftje, G.M.: Recent advances in detector-array technology for mass spectrometry. *Int. J. Mass Spectrom.* **238**(1), 33–46 (2004)
9. Koppelaar, D.W., Barinaga, C.J., Denton, M.B., Sperline, R.P., Hieftje, G.M., Schilling, G.D., Andrade, F.J., Barnes, J.H. IV: MS Detectors. *Anal. Chem.* **77**(21), 418 A–427 A (2005)
10. Geno, P.W., Macfarlane, R.D.: Secondary electron emission induced by impact of low-velocity molecular ions on a microchannel plate. *Int. J. Mass Spectrom. Ion Process.* **92**, 195–210 (1989)
11. Gilmore, I.S., Seah, M.P.: Ion detection efficiency in SIMS: Dependencies on energy, mass and composition for microchannel plates used in mass spectrometry. *Int. J. Mass Spectrom.* **202**(1–3), 217–229 (2000)
12. McClenathan, D.M., Hieftje, G.M.: Absolute methods of quantitation in glow discharge mass spectrometry with a time-of-flight mass analyzer. *J. Anal. At. Spectrom.* **20**(12), 1326–1331 (2005)
13. Myers, D.P., Li, G., Mahoney, P.P., Hieftje, G.M.: An inductively coupled plasma-time-of-flight mass spectrometer for elemental analysis. Part II: Direct current quadrupole lens system for improved performance. *J. Am. Soc. Mass Spectrom.* **6**(5), 400–410 (1995)
14. Rogers, D.A., Ray, S.J., Hieftje, G.M.: An electrospray/inductively coupled plasma dual-source time-of-flight mass spectrometer for rapid metallomic and speciation analysis: instrument design. *Metallomics* **1**(1), 67–77 (2009)
15. Dawson, J.H.J., Guilhaus, M.: Orthogonal-acceleration time-of-flight mass spectrometer. *Rapid Commun. Mass Spectrom.* **3**(5), 155–159 (1989)
16. Cotter, R.J.: *Time-of-flight mass spectrometry*, vol. 549. American Chemical Society, Washington DC (1994)
17. Birkinshaw, K.: Fundamentals of focal plane detectors. *J. Mass Spectrom.* **32**(8), 795–806 (1997)
18. Schilling, G.D., Ray, S.J., Rubinshtein, A.A., Felton, J.A., Sperline, R. P., Denton, M.B., Barinaga, C.J., Koppelaar, D.W., Hieftje, G.M.: Evaluation of a 512-channel Faraday-strip array detector coupled to an inductively coupled plasma Mattauch Herzog mass spectrograph. *Anal. Chem.* **81**(13), 5467–5473 (2009)
19. Barnes, D., Sperline, R., Denton, M.B., Barinaga, C.J., Koppelaar, D., Young, E.T., Hieftje, G.M.: Characterization of a focal plane camera fitted to a Mattauch Herzog geometry mass spectrograph. I. Use with a glow-discharge source. *Anal. Chem.* **74**(20), 5327–5332 (2002)
20. Burgoyne, T.W., Hieftje, G.M., Hites, R.A.: Design and performance of a plasma-source mass spectrograph. *J. Am. Soc. Mass Spectrom.* **8**(4), 307–318 (1997)
21. Knight, A.K., Sperline, R.P., Hieftje, G.M., Young, E., Barinaga, C. J., Koppelaar, D.W., Denton, M.B.: The development of a micro-Faraday array for ion detection. *Int. J. Mass Spectrom.* **215**(1–3), 131–139 (2002)
22. Barnes, J.H., Schilling, G.D., Sperline, R.P., Denton, M.B., Young, E. T., Barinaga, C.J., Koppelaar, D.W., Hieftje, G.M.: Coupling of a gas chromatograph to a simultaneous-detection inductively coupled plasma mass spectrograph for speciation of organohalide and organometallic compounds. *J. Anal. At. Spectrom.* **19**(6), 751–756 (2004)
23. Ardel, D.: First Results with a New Multichannel Ion Detector. Paper presented at the 2010 Winter Conference on Plasma Spectrochemistry, 6 January 2010.